Research paper

Cosmogenic nuclide surface exposure dating of boulders on last-glacial and late-glacial moraines, Lago Buenos Aires, Argentina: Interpretive strategies and paleoclimate implications

D.C. Douglass[a,*], B.S. Singer[a], M.R. Kaplan[b,a], D.M. Mickelson[a], M.W. Caffee[c]

[a]*Department of Geology and Geophysics, University of Wisconsin-Madison, 1215 W. Dayton St., Madison, WI 53706, USA*
[b]*School of GeoSciences, University of Edinburgh, Scotland, UK*
[c]*PRIME Lab, Purdue University, West Lafayette, IN 47907, USA*

Abstract

In situ cosmogenic nuclides have become a powerful means to determine surface exposure ages of boulders on moraines and other landforms that are important to paleoclimate reconstructions. Potentially the largest and least quantifiable source of uncertainty of these surface exposure ages is the variable exposure histories of individual boulders. We use the mean square of weighted deviates (MSWD) statistic and cumulative frequency plots to identify groups of boulders that have statistically similar ages based on the number of analyses and their uncertainties. These samples most likely represent the true age of the moraine. We use these tools to interpret 49 ^{10}Be and ^{26}Al surface exposure ages of erratic boulders on six last-glacial and late-glacial moraines at Lago Buenos Aires, Argentina (LBA; 71°W, 46.5°S). Seven of the 49 boulders are identified as anomalously young, and are interpreted to have been exhumed after moraine deposition. The remaining 42 samples indicate that glacial advances or still-stands of the ice margin occurred at 22.7 ± 0.9, 21.4 ± 1.9, 19.9 ± 1.1, 17.0 ± 0.8, 15.8 ± 0.6, and 14.4 ± 0.9 ka (weighted mean ages $\pm 2\sigma$, analytical, erosion rate, and attenuation length uncertainties). This chronology of an outlet of the Patagonian Ice Cap is comparable to many records in the Northern Hemisphere despite a maximum in local summer insolation during this period. The implication is that climate during the Last Glacial Maximum was generally synchronous at the global scale. However, the late-glacial readvance to 95% of the extent of the largest advance during the Last Glacial Maximum at 14.4 ± 0.9 ka is distinctively "Antarctic" in nature. It is contemporaneous with the Antarctic Cold Reversal, and precedes the Younger Dryas Chronozone. Further, our precise exposure ages highlight climatic asynchrony across southern South America between 23 and 14 ka. The timing of maximum ice extent and onset of deglaciation at LBA occurred ~4 ka later than in the northern parts of the Chilean Lake District (41°S), but were synchronous with glacial advances or still stands in the Strait of Magellan (52°S). This regional asynchrony is likely related to the strength and position of the Southern Westerlies.
© 2006 Elsevier Ltd. All rights reserved.

Keywords: Paleoclimate; Glacial chronology; Cosmogenic nuclide surface exposure dating; Beryllium-10; Aluminum-26; Antarctic cold reversal; Lago Buenos Aires; Argentina

1. Introduction

In-situ cosmogenic nuclide dating of glacial deposits has emerged as a powerful means of revealing precise chronological information crucial to regional and global reconstructions of past climate (e.g., Gosse et al., 1995; Owen et al., 2003; Licciardi et al., 2004; Douglass et al., 2005). A distinct advantage of the cosmogenic nuclide surface exposure method is that moraine deposition is directly dated, but a host of analytical and geological factors can introduce uncertainties to the interpreted age. Other chronometers, such as radiocarbon dating, may have fewer systematic uncertainties, but because the ages are those of organic material that is either stratigraphically older or younger than the landform, precision is also highly

*Corresponding author. Present address: Department of Earth and Environmental Sciences, Northeastern University, 360 Huntington Ave., Boston, MA 02115, USA. Tel.: +1 617 373 4381; fax: +1 617 373 4378.
 E-mail address: d.douglass@neu.edu (D.C. Douglass).

dependent on the closeness of this bracketing. For example, 13 minimum ages for retreat after glacial stage "D" in the Strait of Magellan range between $14,455 \pm 230$ and $13,050 \pm 190$ ^{14}C a BP ($\pm 2\sigma$; McCulloch et al., 2005b). Some interpretation is required to determine which sample(s) best represent the timing of deglaciation. Where both minimum and maximum ages are available, plausible age ranges may be up to several thousand years. Moreover, in many semi-arid and polar tundra environments, datable organic material is unavailable, rendering any effort with radiocarbon impossible.

The uncertainty of a cosmogenic nuclide-based age of a glacial-geomorphic feature comprises at least four components. First, analytical uncertainties associated with isotope dilution and accelerator mass spectrometry (AMS) are typically 2–5%, but may be higher for samples with low isotope concentrations (Gosse and Phillips, 2001). These errors have improved with the development of better sample-processing procedures and more efficient and sensitive accelerator mass spectrometers (Finkel and Suter, 1993). Second, production rates of cosmogenic isotopes are uncertain because of the limited number and distribution of calibration sites and neutron flux monitors that are used to determine empirically the scaling factors that describe the production variation with latitude and elevation. The magnitude of this uncertainty is poorly constrained but estimated to be less than 10–20% (Gosse and Phillips, 2001). The CRONUS (Cosmic-Ray Produced Nuclide Systematics on Earth) project aims to improve these production rates and scaling factors (Phillips, 2004). Third, the weathering or erosion rate of moraine boulders may be uncertain and difficult, if not impossible, to quantify. Boulder erosion rates can have profound impact on the accuracy and precision of ages for older boulders but are much less significant for samples younger than about 25 ka (Gosse and Phillips, 2001). Lastly, and perhaps most importantly, a host of geological processes can cause large age differences between the youngest and oldest samples on a moraine (Putkonen and Swanson, 2003; Gosse et al., 2003; Kaplan et al., 2005). These geologic processes cause moraine boulders to have variable exposure histories, and include inheritance of isotopes from prior exposures, post-depositional exhumation of boulders, rotation of boulders on moraine surfaces, neutron leakage, partial cover with snow, dust or ash, and several other factors that could cause unusual isotopic concentrations (Bierman et al., 2002).

Of these four types of uncertainties, the variability in exposure history from boulder to boulder is potentially the largest and commonly the most difficult to constrain. Identification of anomalously old or young samples is difficult without a priori knowledge of the landform age, and is only possible if many samples have been analyzed from each landform. Approaches to best estimate the age of a landform include using: (1) the sample that yields the oldest apparent age that is not an obvious outlier (Zreda and Phillips, 1995), (2) the sample that yields the youngest apparent age that is not an obvious outlier (Benson et al., 2005), (3) the arithmetic mean and standard deviation (Ivy-Ochs et al., 1999), or (4) the inverse-variance weighted mean of the ages (Douglass et al., 2005). Regardless of the approach used, the inclusion or exclusion of samples should be based on robust statistical methods whenever possible. This paper reviews two methods that can be used to identify geologic outliers and calculate moraine ages, using a large set of ^{10}Be and ^{26}Al exposure ages from near Lago Buenos Aires (LBA), Argentina (71.0°W, 46.5°S; Fig. 1, inset), as an example.

Whether cooling events during the Younger Dryas (YD) Chronozone or the Antarctic Cold Reversal (ACR) affected southern South America is highly controversial (Sugden et al., 2005). The majority of paleoclimate information comes from pollen records. For example, pollen abundances in sediment cores from the Chilean Lake District (CLD) at 41°S (Fig. 1 inset; Moreno et al., 2001), and an increase in fine silt in nearby Lago Mascardi (Fig. 1 inset; Ariztegui et al., 1997; Hajdas et al., 2003), support a late glacial cooling that begins prior to, and ends contemporaneously with, the YD. In contrast, pollen records from the Taitao Peninsula and nearby islands show no sign of climate change during this interval (Fig. 1 inset; Bennett et al., 2000), and those from the Strait of Magellan region are equivocal (Fig. 1 inset; see the contrasting interpretations of pollen from Puerto del Hambre; Heusser et al., 2000; McCulloch and Davies, 2001). Moraines thought to correspond to the YD have been dated using radiocarbon (Mercer, 1968, 1976; Marden and Clapperton, 1995; Wenzens, 1999; Strelin and Malagnino, 2000), but the small number of dates and the loose stratigraphic bracketing do not constrain moraine ages with sufficient precision to provide unequivocal evidence that glaciers advanced in southern South America during the YD and/or the ACR.

We develop a precise chronology for six moraines deposited during the last glaciation to address a fundamental question in paleoclimate research: Are climate changes synchronous at global and regional scales? This has been debated for the better part of two decades. Several studies have used the nearly global distribution of cooling events like the YD (e.g., Steig et al., 1998) as an indication that climate changes are rapidly propagated across the Earth, either by external solar forcing (e.g., Bond et al., 2001) or by changing concentrations of greenhouse gases in the atmosphere such as water and/or carbon dioxide (e.g., Cane and Clement, 1999; Brook et al., 1999). Others have argued that these rapid climate changes are initiated in the ocean by changes in the global thermohaline circulation system (e.g., Broecker and Denton, 1989). Reconstructing the Earth's climate system at regional and global scales using a large number of temporally precise paleoclimate records with global spatial coverage is one way these hypotheses can be evaluated (e.g., Denton et al., 1999a).
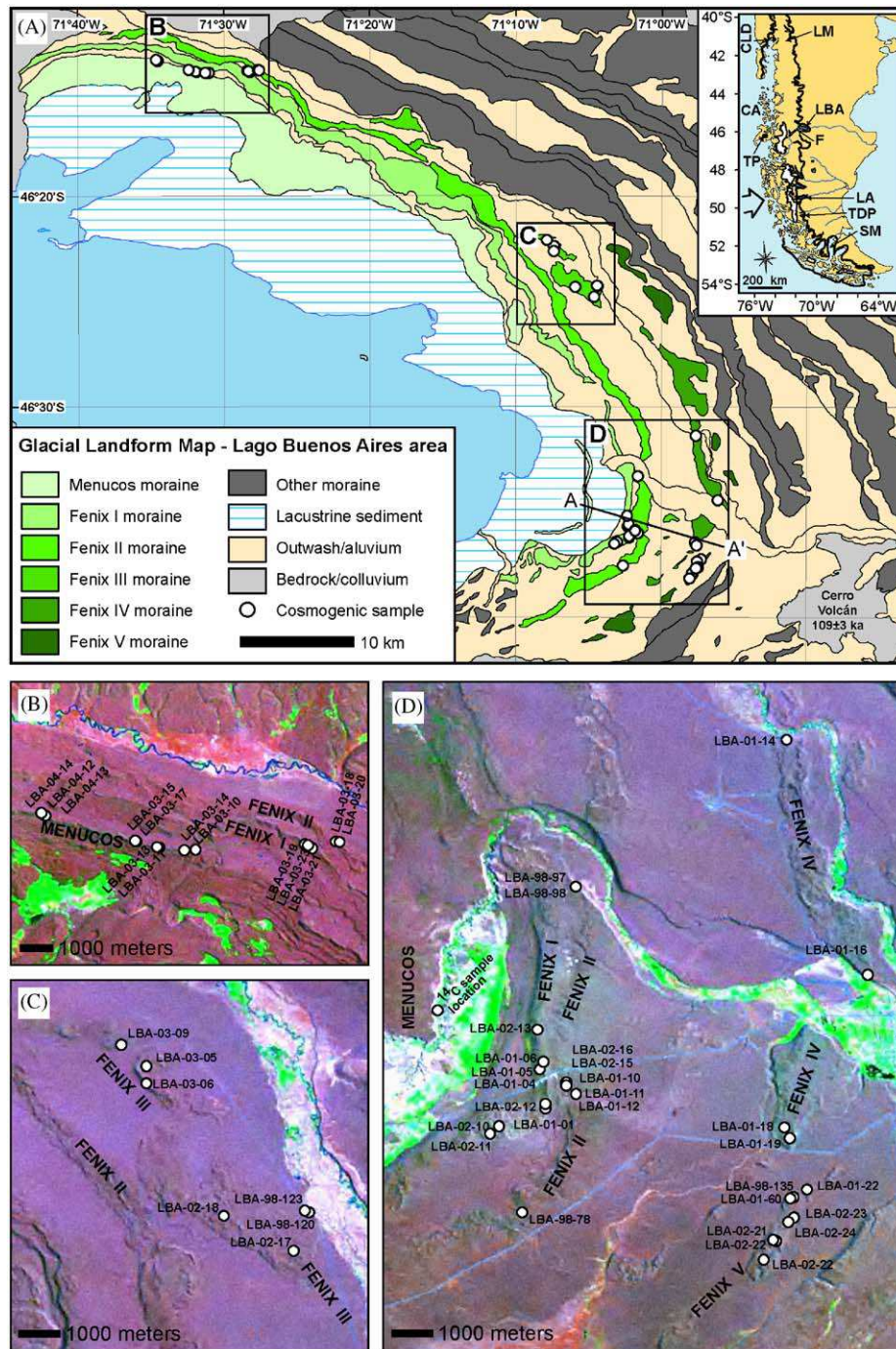
Fig. 1. (A) Glacial landform map of Lago Buenos Aires region, Argentina. A–A′ depicts location of topographic cross-section shown in Fig. 2. Location figure in inset: heavy black line marks the margin of the Patagonian Ice Cap at the Last Glacial Maximum; the modern ice caps are shown in white. CLD—Chilean Lake District, LM—Lago Mascardi, CA—Chonos Archipelago, LBA—Lago Buenos Aires, F—Fachinal, TP—Taitao Peninsula, LA—Lago Argentino, TDP—Torres del Paine, SM—Strait of Magellan. (B), (C), and (D) Landsat images and sample locations for the three main sampling areas.

2. Geologic Setting

The moraine sequence at LBA, in the semi-arid plain east of the Southern Andes and the North Patagonia Ice Field, is a well-preserved archive of glacial fluctuations over the last million years (Fig. 1; Caldenius, 1932; Singer et al., 2004). The six moraines from the last glaciation are informally named Fenix V (oldest) through Fenix I and Menucos (youngest) (Fig. 2; Kaplan et al., 2004). Fenix III, IV, and V have been crosscut by younger outwash, but the preserved segments of the moraines are hummocky, which we interpret as primary glacial topography, and are up to 1.5 km wide (Fig. 3A). Fenix II and I are nearly continuous single-crested ridges about 0.5 km wide. The Menucos
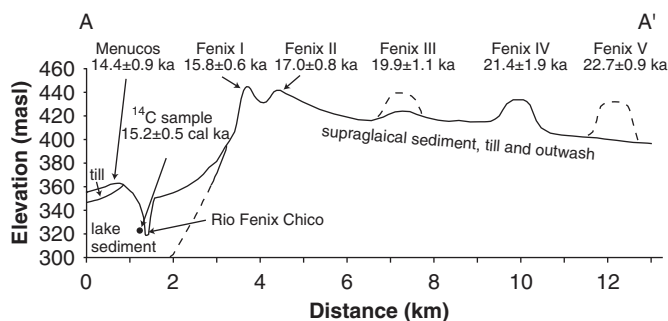
Fig. 2. Topographic cross-section across last-glacial moraine sequence. Fenix III and Fenix V are not preserved at the exact location of the cross-section and are sketched in with dashed lines. The stratigraphic relationship between the Menucos moraine, the carbonate concretion-bearing lake sediments, and the Fenix I moraine is clearly shown.

moraine is also sharp and single-crested, and is best preserved on the north side of the valley (Fig. 3B). It is not as prominent in the center of the valley, where the glacier terminated in a proglacial lake, but is preserved as a low ridge of till surmounted by large basaltic blocks several meters in diameter that rest directly upon varved lacustrine sediments (Fig. 2). This is the youngest preserved moraine east of LBA; however, additional Holocene moraines are located 90 km further to the west, at Fachinal, Chile (Douglass et al., 2005). Carbonate concretions from the upper portions of a sequence of lake sediments that lies stratigraphically between the Fenix I and Menucos moraines gave an AMS date of $12,880 \pm 320$ [14]C a BP ($\pm 2\sigma$; Kaplan et al., 2004; 15.2 ± 0.5 calibrated ka BP (cal ka)[1]; Fig. 2). There are carbonate-bearing pre-Quaternary bedrock units in this valley, so it is possible that some amount of "dead" carbonate present in pore fluids was incorporated into these concretions during their growth. Thus, the lake sediments could be younger than 15.2 ± 0.5 cal ka, but not older. Nevertheless, this AMS radiocarbon age provides an independent constraint that limits the uncertainty of cosmogenic nuclide production rates used in this study (see Section 5.2).

3. Methods

Organic material suitable for radiocarbon dating was not found in the moraines; consequently, the timing of deposition is determined by measuring the concentrations of in situ cosmogenic [10]Be (and [26]Al in some cases) in 49 erratic boulders (e.g., Figs. 3C–F). Samples were collected by hand with hammer and chisel from large (0.3–2.75 m diameter) boulders at or near each moraine crest. The preferred boulder is one that has a wide flat surface that can be easily sampled, does not appear to have moved, or

be weathering quickly, and has 20–30% quartz. Lithologies sampled were generally granitoid, but also included quartz-bearing rhyolites, sedimentary, and metamorphic rocks. Some rocks were slightly weathered, but many preserved glacial sculpting or polish. The position and elevation of the samples was determined with a global positioning system (GPS) and digital barometric altimeter, respectively. There was good agreement between the altimeter and GPS elevations and we estimate a precision of ± 10 m. Horizon shielding was characterized by several clinometer measurements, but corrections are minor (see below).

3.1. Chemical processing of samples

Chemical isolation of [10]Be and [26]Al was performed at the University of Wisconsin-Madison following the methods of Bierman et al. (2002), with minor variations for some of the samples. Up to 100 g of quartz was separated from 1 to 2 kg of crushed rock by mechanical (magnetic and heavy liquid separation) and chemical (acid dissolution of non-quartz minerals) procedures. The quartz was repeatedly etched in a dilute solution of nitric and hydrofluoric acid to remove the outer rim of the quartz crystals and any meteoric [10]Be. After cleaning and a test by ICP-AES to verify quartz purity, i.e., total Be at background levels ($\sim 0\,\mu g$) and total Al at or below 5 mg, between 13 and 55 grams of quartz was dissolved in a mixture of concentrated HF and HNO_3, along with a 500 μg spike of beryllium standard (Spex CertiPrep—Claritas PPT^{TM}). Additional aluminum standard was added to some samples to ensure there was at least 2000 μg of total aluminum. A procedural blank for each batch of 11 samples is used to determine the amount of contaminant, non-cosmogenic [10]Be and [26]Al contained in the spike, reagents, exchange resins, and vessels used in sample processing. After dissolution, beryllium and aluminum were isolated from other trace impurities in the quartz through a series of selective chemical precipitations, as well as cation and anion exchange column separations. The beryllium and aluminum were oxidized, mixed with niobium or silver metal, respectively, and packed into a target for AMS analysis (Muzikar et al., 2003 and references therein).

Most AMS analyses for [10]Be were performed at PRIME Lab, Purdue University; however, the samples described in Kaplan et al. (2004) were measured at CAMS, Lawrence Livermore National Laboratory. At PRIME Lab, [10]Be was measured against standards derived from NIST SRM 4325, and we accordingly increase ratios by 14% (keeping percent error constant) to correct for activity differences between this standard and those used at other AMS facilities (see note 34 in Partridge et al. (2003)). As cosmogenic isotope production rates are determined empirically, knowledge of the exact activity of [10]Be is not necessary as long as there is robust intercalibration between standards (the basis of the 14% correction). [10]Be and [26]Al concentrations in the quartz were determined by isotope dilution calculations. Total beryllium is determined

---

[1]These and all radiocarbon dates have been calibrated with the IntCal04 dataset (Reimer et al., 2004) if younger than 26 cal ka, and the CALPAL_2004Jan dataset (Weninger et al., 2004) if older than 26 cal ka. Uncertainties of all radiocarbon and cosmogenic ages are reported at $\pm 2\sigma$ with only analytical contributions.
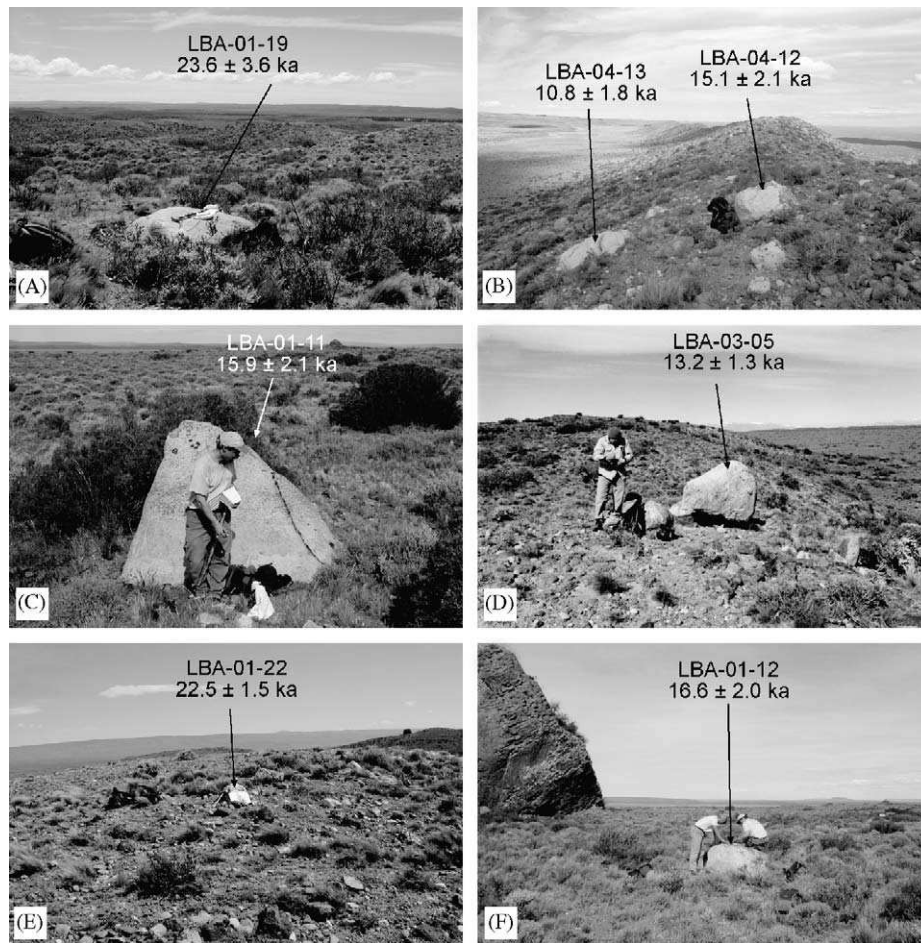
Fig. 3. Field photos of moraine crests and erratic boulders. (A) Crest of the broader, more-hummocky Fenix IV moraine with a sampled boulder. (B) Ice-distal side of the sharp-crested Menucos moraine with two boulders. Note the age differences despite their close proximity. (C) Sample LBA-01-11 on Fenix II. D. Sample LBA-03-05 on Fenix III. Despite the large size of this sample, its age was anomalously young. (E) Sample LBA-01-22 on Fenix V. Despite the small size of this sample (32 cm tall), its age was very similar to the weighted-mean age of this moraine. (F) Sample LBA-01-12 on Fenix II.

from the amount of spike added to the sample and total aluminum is determined from an ICP-AES measurement of aluminum concentration in an aliquot taken after sample dissolution. The blank correction averaged 5% (1–14%), and was made by subtracting the blank ratio from the sample ratio.

3.2. Data reduction

Cosmogenic nuclide surface exposure ages were calculated using

$$t = \frac{-1}{\lambda + E/L} \left[\ln\left(1 - \frac{N}{P}(\lambda + E/L)\right) \right], \qquad (1)$$

where t is the duration of exposure (years), N the concentration of the nuclide (atoms g^{-1}), P the production rate (atoms g^{-1} y^{-1}), λ the decay constant (4.56×10^{-7} and 9.8×10^{-7} y^{-1} for ^{10}Be and ^{26}Al, respectively; Holden, 1990), E the erosion rate (see below; assuming a rock density of 2.7 g cm^{-3}), and L the rate at which cosmic rays are attenuated with depth (145 g cm^{-2} for ^{10}Be and 156 g cm^{-2} for ^{26}Al; Brook et al., 1996). We use the

production rates and scaling factors in Stone (2000). Multi-decadal climate records in the region are sparse, but we estimate that mean annual sea level temperature is 281 K and the mean annual sea level pressure is 1009.3 mb (National Center for Atmospheric Research, 2003). A correction for modulation of production rate by changes in paleomagnetic field intensity follows Nishiizumi et al. (1989) using the SINT-800 record (Guyodo and Valet, 1999). The production rate is then scaled for sample thickness according to Eqs. 3.78 and 3.81 of Gosse and Phillips (2001), and topographic shielding according to Eq. 6 of Dunne et al. (1999). We do not apply a correction for snow cover as the winter snow pack is currently thin and short-lived (area land owners, pers. comm., 2001). Also, we do not apply corrections for boulder geometry or shape. There is no vegetative shielding in this environment. None of these corrections have significant impacts on the resulting ages. The exposure ages presented assume a boulder weathering or erosion rate of 1.4 ± 1.2 mm/kyr ($\pm 2\sigma$; Kaplan et al., 2005). This rate is determined from measurements of ^{10}Be and ^{26}Al concentrations in boulders on moraines known to be 760–1016 ka based on

stratigraphic relationships to $^{40}Ar/^{39}Ar$-dated basalt flows in the area (Singer et al., 2004). Zero erosion rate exposure ages of these samples range between ca.100 and ca.450 ka, but assuming erosion rates 0.8–2.2 mm/kyr increases their apparent exposure ages to the correct age. Including boulder weathering in the data reduction does not significantly impact these ages; ^{10}Be boulder exposure ages and uncertainties generally increase by about 2% and 6%, respectively.

Uncertainties are calculated according to the General Rule presented in Taylor (1997; equation 3.47; partial differential of Eq. (1) with respect to each of the variables) and includes analytical uncertainty in the isotope concentration measurement (N in Eq. (1); weighing of sample, weighing and concentration of spike, and AMS counting statistics), as well as erosion rate (E in Eq. (1)) and attenuation length uncertainty (L in Eq. (1)). All age uncertainties are reported at the 95% confidence level. Uncertainties in production rates were not explicitly treated in the data reduction. Although the latter are generally poorly constrained and thought to be less than 10–20% (Gosse and Phillips, 2001), the independent comparison between surface exposure and AMS radiocarbon ages at LBA and local calibration sites suggest it is unlikely that local production rate uncertainties for ^{10}Be and ^{26}Al exceed 10% (see Section 5.2).

3.3. Identification of outliers and moraine ages

Given the potential sources of uncertainty in cosmogenic nuclide surface exposure dating of moraines, it is commonly necessary to obtain apparent ages from several boulders on a single moraine and pool results to constrain as precisely as possible the time elapsed since deposition (e.g., Gosse et al., 1995, Licciardi et al., 2004; Douglass et al., 2005). There are three main mechanisms that introduce geologic uncertainty and lead to a spread in apparent cosmogenic nuclide surface exposure ages beyond what is expected from analytical sources of uncertainty. First, partial burial of the boulder by snow, ash, or dust will cause exposure ages to be younger than the true age of the moraine. Second, isotopes inherited due to exposure of boulder surfaces to cosmic rays prior to deposition on the moraine surface will produce anomalously old apparent exposure ages. Third, there are a host of processes that may cause boulders to be exhumed after deposition within a moraine. In the few hundred to few thousand years after deposition, the melting of buried ice within a moraine could lead to instability causing boulders to be exhumed. In the longer term, erosion of the surrounding sediment might exhume boulders long after moraine deposition, or cause boulders already at the surface to rotate or shift position exposing a new surface of the boulder. Frost-heave might also push boulders to the surface of the moraine in some environments.

To determine a precise and accurate age for the moraine, we need to differentiate between those samples which accurately reflect the time of deposition and others that have unusual exposure histories. In our analysis, we assume that many of the boulders currently at the moraine surface record the timing of the last deposition on the moraine crest, and that these boulders were deposited over a short time interval relative to the magnitude of the analytical uncertainties associated with these age determinations (i.e., less than 1 ka). We also assume that some boulders may contain isotopes inherited from a prior exposure, and that other boulders currently at the surface may originally have been buried and were later exhumed. Accordingly, if many boulders are sampled, a few may have ages that are unusually old or young, but a group of samples that represent the depositional age of the moraines will share a common age and exhibit some degree of central tendency.

Therefore, we need to test whether all data from a moraine are sampling a common mean value. The approach of McIntyre et al. (1966) has become widely used in radioisotopic geochronology (e.g., Dalrymple and Lanphere, 1969; McDougall and Harrison, 1999, p. 135). In this method, outliers are identified with the mean square of weighted deviates (MSWD) statistic, and average ages are calculated with the inverse-variance weighted mean. Following this approach, we combine the MSWD with cumulative probability curves (Deino and Potts, 1992) to identify a group of samples that share a common mean age and infer that this gives the time since moraine formation. Data from boulders that give apparent exposure ages which do not coincide with the common mean age are excluded. The MSWD compares the observed variability within the sample population to the expected variability defined by the analytical uncertainties of the measurements, and is equivalent to the χ^2 statistic divided by the number of degrees of freedom (n–1 in this case):

$$MSWD = \frac{\sum [(t_i - T_{moraine})^2/(\sigma_i)^2]}{n - 1},$$ (2)

where t_i is the age of an individual analysis, $T_{moraine}$ the moraine age (see below), σ_i the uncertainty associated with an individual analysis, and n the number of samples analyzed.

An MSWD value of 1.0 indicates that analytical errors are as expected, whereas a value less than 1.0 indicates that the analytical errors may be overestimated. Alternatively, a value significantly larger than 1.0 indicates that that either analytical errors are underestimated, or that geological factors may be important in producing dispersed exposure ages. The significance of the MSWD value is evaluated by converting it to a χ^2 statistic and determining the appropriate probability limits from tables. A probability value less than 0.05 indicates that there is a significant amount of non-analytical error in the data, and that one or more of the samples are outliers that reflect unusual geological processes. In these cases, the cumulative frequency plots are bimodal, with the secondary peak clearly identifying the outlier(s). These outliers are

excluded from the remaining data and the MSWD is recalculated and re-evaluated. This process continues until the probability value returned exceeds 0.05, indicating that observed age distribution can be explained by the analytic errors alone. However, if the probability values are greater than 0.05 and the MSWD is greater than 1.0, then it remains a possibility that minor non-analytical errors persist, but these are no longer statistically significant. Even though it is possible to continue to exclude samples from the data until the MSWD is less than or equal to 1.0 (the level at which there should be no additional non-random variability in the data), we chose not to utilize such an aggressive and interpretive approach.

We calculate the age of a moraine with the exposure ages that remain in the data, using the inverse-variance weighted mean:

$$T_{\mathrm{moraine}} = \frac{\sum(w_i t_i)}{\sum w_i},\qquad(3)$$

where t_i is the age of each sample and w_i is the weighting factor equivalent to the inverse of the square of the variance of the sample $(1/\sigma_i^2)$. The uncertainty in T_{moraine} is determined as follows: if MSWD < 1.0, then $\sigma_{T_{\mathrm{moraine}}} = 1/\sum w_i$; if MSWD > 1.0 then $\sigma_T = \sqrt{\mathrm{MSWD}} \times \sqrt{1/\sum w_i}$. This additional term estimates the non-significant amount of non-random error that may remain in such data.

We prefer the inverse-variance weighted mean as the best estimate of moraine age for several reasons. First, following the exclusion of geologic outliers, the remaining uncertainty should be mostly analytical rather than geologic. Therefore, it is reasonable to weight the importance of a sample according to the quality of its measurement (McIntyre et al., 1966; McDougall and Harrison, 1999). In this way, more precisely measured samples have more leverage on the resulting age than those which are less well measured; the latter are commonly relatively small samples with low concentrations of cosmogenic nuclides. Second, the information about the analytical uncertainties associated with each sample is not preserved in a simple arithmetic mean calculation, where the uncertainty is determined by the standard deviation of the sample population. As a hypothetical example, taking the arithmetic mean of a group of analyses that have similar ages, but large uncertainties, will lead to a very low standard deviation and a possible underestimation of the actual uncertainty in the age of the landform. The calculation of the inverse-variance weighted-mean age and the MSWD statistic, the χ^2 test, and the generation of the cumulative frequency curves were performed with Isoplot/Ex, an Excel add-in program written by and available from Ken Ludwig (2003).

For comparison, we also calculate ages for the moraines by the arithmetic mean, the youngest and oldest sample, as well as the peak in the cumulative frequency curve. In the case of the arithmetic mean, we calculate moraine ages two ways. First, using all of the samples (i.e., excluding no

outliers), and second, excluding outliers with the same MSWD and χ^2 approach described above, but using the arithmetic instead of the inverse-variance weighted mean as T_{moraine}.

4. Results

Boulder information and details about sample chemistry are presented in Table 1. Eleven of the samples were originally presented in Kaplan et al. (2004), and were analyzed at LLNL. The remaining 38 samples were analyzed at PRIME Lab. LBA-98-98 is not used in moraine age calculations because the ^{10}Be and ^{26}Al ages do not agree within analytical uncertainties. The replicate ^{10}Be analyses for samples LBA-03-14 and LBA-03-05 are in good agreement with each other.

Based on our statistical approach, seven of the 49 boulders (14%) have anomalously young ages and are identified as geologic outliers using the χ^2 and cumulative frequency method (hollow symbols, Fig. 4). We interpret these boulders as having been exhumed after deposition, but it is possible that the boulders have shifted or rotated. It is unlikely that snow cover is a significant factor in this environment as the winter snow pack is generally thin and short-lived. Also, the samples were collected from ridges on the moraines, which are likely to be windswept and have less snow. It is also unlikely that these samples have been affected by ash or dust cover. The 10 cm of ash deposited here after the 1991 eruption of Volcán Hudson (Inbar et al., 1995) has almost been completely removed from the region in 15 years by the strong and persistent wind.

No samples were identified as anomalously old; however, one sample from Fenix III, two from Fenix IV, and one from Fenix V do cause slight shoulders on the older side of the cumulative frequency curves (Figs. 4D–F). These slightly older ages may be the result of a small amount of inheritance from prior exposure; alternatively these older samples may represent the true age of the moraine if all other samples were exhumed after deposition. The merits of these two interpretations are discussed below.

The weighted-mean ages for the six moraines based on 42 samples are 22.7 ± 0.9, 21.4 ± 1.9, 19.9 ± 1.1, 17.0 ± 0.8, 15.8 ± 0.6, and 14.4 ± 0.9 ka. These age determinations are characterized by MSWD values between 0.8 and 2.2—within the range expected for 4–10 samples from each moraine (Fig. 4; Table 2). These new age determinations refine those published in Kaplan et al. (2004). The moraine-age uncertainties have decreased by about 65%, and we also present ages for two additional moraines (Menucos and Fenix IV).

For all moraines, the arithmetic and weighted-mean ages of the moraines are nearly identical (Table 2), but the weighted-mean ages are more precise. Using the arithmetic mean age for T_{moraine} in the MSWD and χ^2 analysis (Eq. (2)) leads to the exclusion of nine outliers (eight young and one old). The differences between the oldest samples and the weighted-mean ages are between 1 and 2.3 ka,

Table 1
Cosmogenic [10]Be and [26]Al surface exposure data from 49 boulders

Sample ID	Lithology	Boulder height (m)	Boulder diam. (m)	Thickness (cm)	Lat. (°S)	Long. (°W)	Altitude (m asl)	Mass quartz (g)	Isotope and Lab[a]	Isotope conc.[b,c] (10^4 at g^{-1} ±2σ)	Prod. rate (at g^{-1} yr^{-1})	Exposure age ±2σ ka
MENUCOS												
LBA-03-10	Granite	1.50	1.75	3	46.236	71.516	628	47.439	Be-P	11.8±1.1	8.98	13.4±2.5
LBA-03-11	Granite	0.30	1.10	2.5	46.236	71.530	651	47.946	Be-P	14.2±2.7	9.18	15.9±6.3
LBA-03-13	Rhyolite	0.80	1.05	3	46.236	71.531	656	35.271	Be-P	13.5±0.9	9.20	15.0±2.2
LBA-03-14	Granite	0.40	1.00	3	46.236	71.521	646	51.174	Be-P-A	8.2±0.6	9.12	9.1±1.3
								41.491	Be-P-B	9.6±0.6	9.12	10.7±1.4
LBA-03-15	Granite	0.65	0.80	3.5	46.234	71.539	673	46.132	Be-P	9.9±0.8	9.29	10.8±1.8
LBA-03-17	Granite	0.90	1.50	3	46.234	71.540	673	51.123	Be-P	11.9±0.8	9.33	13.1±1.8
LBA-04-12	Granite	0.45	0.85	2	46.227	71.575	722	39.533	Be-P	14.5±1.0	9.80	15.1±2.1
LBA-04-13	Granite	0.40	1.00	2	46.227	71.575	722	55.234	Be-P	10.5±0.6	9.80	10.9±1.4
LBA-04-14	Granite	1.35	2.00	2.5	46.226	71.577	737	47.259	Be-P	14.5±0.8	9.88	15.0±1.8
FENIX I												
LBA-01-01	Granite	1.15	1.20	1.5	46.604	71.036	445	32.880	Al-L	61.0±16	47.8	13.0±7.2
LBA-01-04	Granite	0.30	0.50	3	46.595	71.038	438	38.572	Be-P	12.5±0.7	7.67	16.7±1.9
LBA-01-05	Conglom	0.30	1.25	1.5	46.595	71.038	438	31.720	Be-L	11.7±0.4	7.78	15.4±1.2
								31.720	Al-L	101±23	47.5	22.1±11
LBA-01-06	Granite	1.00	1.30	1.5	46.594	71.036	438	13.230	Be-L	13.7±1.1	7.78	18.1±3.0
								13.230	Al-L	62.1±8.2	47.5	13.4±3.6
LBA-02-10	Granite	0.50	1.00	3	46.608	71.050	428	27.557	Be-P	11.8±0.7	7.61	15.9±1.9
LBA-02-11	Granite	0.50	0.75	3	46.609	71.053	420	19.404	Be-P	12.4±1.0	7.56	16.9±2.9
LBA-02-12	Granite	0.60	1.00	3	46.603	71.036	432	14.979	Be-P	10.8±1.2	7.63	14.4±3.4
LBA-02-13	Granite	0.50	0.75	3	46.587	71.038	444	21.049	Be-P	11.2±1.5	7.72	14.8±4.1
LBA-03-19	Rhyolite	0.50	1.35	3	46.235	71.473	699	39.871	Be-P	13.0±0.9	9.57	13.8±2.0
LBA-03-21	Granite	0.45	0.85	3	46.236	71.470	699	41.992	Be-P	9.5±0.9	9.57	10.1±2.0
LBA-03-23	Granite	0.75	1.20	3	46.235	71.472	700	39.205	Be-P	15.6±1.0	9.57	16.7±2.1
FENIX II												
LBA-98-78	Granite	0.60	1.20	1.5	46.626	71.043	454	25.580	Be-L	13.5±0.5	7.91	17.5±1.5
								25.580	Al-L	97.0±9.0	48.3	20.8±4.1
LBA-98-97	Granite	0.85	1.65	1.5	46.556	71.026	430	15.330	Be-L	13.5±0.6	7.74	18.0±1.6
								15.330	Al-L	82.8±13	47.3	18.1±6.0
LBA-98-98	Granite	0.57	1.20	1.5	46.556	71.026	430	20.530	Be-L	14.7±0.6	7.74	19.6±1.6
								20.530	Al-L	62.0±7.6	47.3	13.4±3.4
LBA-01-10	Rhyolite	0.80	1.25	3	46.598	71.029	445	38.447	Be-P	12.1±0.8	7.74	16.0±2.1

LBA-01-11	Granite	1.50	2.75	3	46.601	71.026	448	47.927	Be-P	12.1±0.8	7.76	15.9±2.1
LBA-01-12	Granite	0.50	1.15	3	46.601	71.026	439	40.949	Be-P	12.4±0.7	7.70	16.6±2.0
LBA-02-15	Granite	0.60	1.30	3	46.598	71.029	435	31.804	Be-P	12.8±0.9	7.67	17.1±2.5
LBA-02-16	Granite	0.75	1.40	3	46.599	71.029	436	25.310	Be-P	13.0±0.8	7.68	17.4±2.2
LBA-03-18	Granite	0.50	0.85	3	46.234	71.461	694	40.179	Be-P	13.6±1.0	9.55	14.5±2.2
LBA-03-20	Granite	0.65	1.00	2	46.234	71.459	709	54.545	Be-P	17.0±1.1	9.76	17.9±2.5
FENIX III												
LBA-98-120	Granite	1.20	1.35	1.5	46.405	71.072	510	11.670	Be-L	17.2±0.7	8.30	21.4±2.0
								11.670	Al-L	133±13	50.7	27.5±5.6
LBA-98-123	Quartzite	0.80	1.00	1.5	46.405	71.073	510	28.570	Be-L	16.7±0.6	8.30	20.7±1.7
								28.570	Al-L	84.0±8.6	50.7	17.1±3.6
LBA-02-17	Granite	1.50	1.50	3	46.414	71.077	485	34.937	Be-P	15.1±0.7	8.01	19.4±2.0
LBA-02-18	Granite	2.50	2.50	3	46.406	71.099	513	47.651	Be-P	15.2±0.8	8.21	19.0±2.2
LBA-03-05	Granite	1.50	1.60	3	46.374	71.123	528	47.735	Be-P-A	10.3±0.7	8.31	12.7±1.8
								49.612	Be-P-B	11.2±0.7	8.31	13.8±1.9
LBA-03-06	Granite	1.60	1.60	1.5	46.377	71.123	532	47.172	Be-P	15.3±1.3	8.46	19.0±2.4
LBA-03-09	Granite	0.65	1.00	3	46.369	71.131	535	45.478	Be-P	14.7±1.0	8.36	18.1±2.5
FENIX IV												
LBA-01-14	Granite	0.30	1.00	3	46.524	70.960	430	31.402	Be-P	14.5±0.8	7.66	19.5±2.3
LBA-01-16	Granite	0.85	1.50	3	46.575	70.934	407	24.580	Be-P	17.1±1.0	7.51	23.6±3.1
LBA-01-18	Rhyolite	0.60	1.15	3	46.608	70.960	430	33.903	Be-P	15.6±0.8	7.66	21.0±2.2
LBA-01-19	Granite	0.50	1.50	3	46.610	70.959	454	37.859	Be-P	17.8±1.3	7.82	23.6±3.6
FENIX V												
LBA-98-135	Granite	0.80	1.00	2	46.623	70.958	439	19.950	Be-L	17.1±0.6	7.80	22.7±1.8
									Al-L	103±22	47.6	22.4±9.9
LBA-01-22	Granite	0.32	0.30	1.5	46.621	70.953	452	22.350	Be-L	17.3±0.6	7.92	22.6±1.7
									Al-L	104±8.9	48.4	22.3±4.0
LBA-01-60	Granite	0.75	1.15	1.5	46.623	70.959	439	25.820	Be-L	18.8±0.8	7.83	25.0±2.2
									Al-L	97.0±13	47.8	21.0±6.0
LBA-02-20	Granite	2.00	2.50	3	46.632	70.963	461	31.410	Be-P	18.0±1.2	7.88	23.6±3.4
LBA-02-21	Granite	0.40	0.65	3	46.632	70.964	468	40.591	Be-P	17.2±1.8	7.93	22.4±5.0
LBA-02-22	Granite	0.65	0.75	2	46.637	70.967	459	29.315	Be-P	14.0±1.0	7.94	18.1±2.7
LBA-02-23	Granite	1.00	1.20	3	46.627	70.957	435	33.270	Be-P	12.5±0.7	7.70	16.6±1.8
LBA-02-24	Granite	0.50	0.85	3	46.628	70.959	435	42.449	Be-P	15.9±0.7	7.70	21.3±2.0

[a]Isotope and lab where analysis was performed: L = CAMS, Lawrence Livermore National Laboratory, P = PRIME Lab, Purdue University. All samples analyzed at CAMS are from Kaplan et al. (2004). [10]Be Replicate analyses for LBA-03-14 and LBA-03-05 are indicated with either an A or B.

[b][10]Be or [26]Al, see isotope column.

[c][10]Be concentrations of samples analyzed at PRIME Lab have been increased by 14% to account for activity differences between PRIME and CAMS standards.
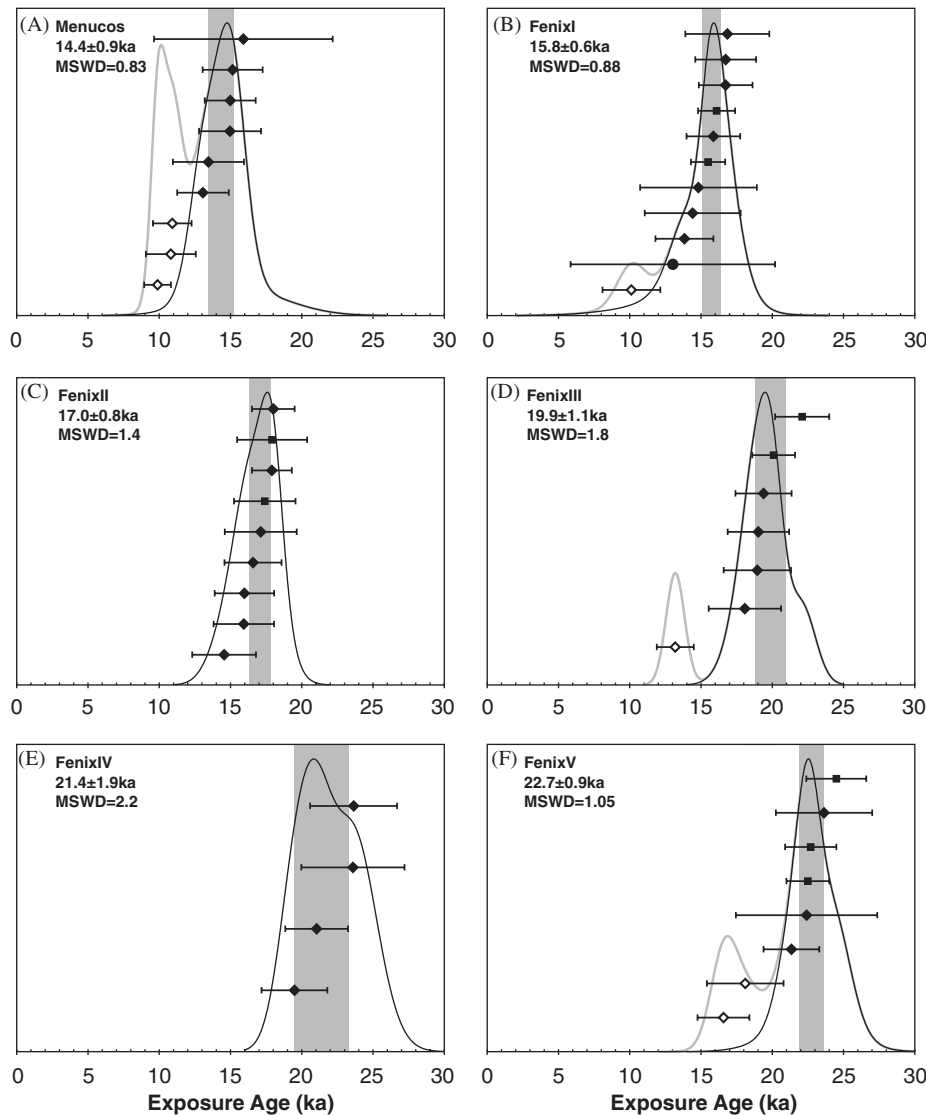
Fig. 4. Cosmogenic surface exposure ages for the six moraines sampled. Each boulder is represented by one symbol and may represent more than one analysis; uncertainties shown at the 95% confidence level. Diamonds represent either single or replicate [10]Be analyses, squares represent [10]Be and [26]Al pairs, and the one circle represents a single [26]Al analysis. Hollow symbols represent outliers. Gray and black cumulative frequency curves represent probability distributions for the total dataset and the dataset without outliers, respectively. Outliers are excluded from the weighted-mean age (vertical gray boxes) and MSWD values for each moraine.

averaging 1.7 ka, but there are no statistically significant differences between the weighted-mean moraine ages and the age of the oldest samples. The youngest boulders are not reliable indicators of moraine age because in two instances these ages contradict the relative stratigraphic ages of the moraines (Fig. 2).

5. Discussion

5.1. A cosmogenic nuclide chronology of glacial to late-glacial ice margins

As with many other cosmogenic nuclide surface exposure studies examining boulder ages from moraines of the last glaciation (cf. Putkonen and Swanson, 2003, and references therein), anomalously young samples are far more prevalent than unusually old samples, suggesting that boulder exhumation is a more widespread problem than inherited isotopes. This is somewhat intuitive. As large ice lobes advanced down-valley tens of kilometers, they eroded the uppermost decimeters to meters of the valley floor (by abrasion and plucking) and valley walls (by mass movement on oversteepened slopes) as well as rounding and abrading away the surfaces of boulders incorporated into the ice, resulting in few boulders with inherited isotopes in the moraines. Yet there are a host of processes that cause boulders to be exposed, rotated, or recovered by additional material once the moraine has been deposited. However, the prevalence of exhumation over inheritance may not be universal. On two moraines at Fachinal, Chile, these same statistical methods indicate that 25% of the samples are anomalously old, which is interpreted to reflect isotope

Table 2
Summary age table

Moraine	Moraine age								Youngest sample	Oldest sample	Frequency maximum
	Arithmethic mean ages				Weighted mean ages						
	All samples	MSWD	Outliers excluded[a]	MSWD	All samples	MSWD	Outliers excluded[b,*]	MSWD			
Menucos	13.2 ± 4.4	10.1	14.6 ± 2.2	0.9	11.9 ± 1.5	7.0	14.4 ± 0.9	0.8	9.9 ± 0.9	15.9 ± 6.3	14.7
Fenix I	14.9 ± 4.0	3.8	15.4 ± 2.6	1.0	15.3 ± 1.1	3.6	15.8 ± 0.6	0.9	10.1 ± 2.1	16.9 ± 2.9	15.8
Fenix II	16.8 ± 2.3	1.4	16.8 ± 2.3	1.4	17.0 ± 0.8	1.4	17.0 ± 0.8	1.4	14.5 ± 2.2	18.0 ± 1.5	17.6
Fenix III	18.7 ± 5.5	14.8	19.1 ± 1.5	0.6	18.0 ± 2.6	14	19.9 ± 1.1	1.8	13.2 ± 1.3	22.1 ± 1.9	19.5
Fenix IV	21.9 ± 4.1	2.4	22.8 ± 3.0	1.5	21.4 ± 1.9	2.2	21.4 ± 1.9	2.2	19.5 ± 2.3	23.6 ± 3.1	20.9
Fenix V	21.5 ± 5.5	7.0	22.9 ± 2.2	1.1	21.3 ± 2.0	7.0	22.7 ± 0.9	1.1	16.6 ± 1.8	24.5 ± 2.1	22.5

Note: all ages given at $\pm 2\sigma$ and include analytical, erosion rate, and attenuation length uncertaintes.
*Preferred moraine age
[a]Outliers include LBA-03-14, LBA-03-15, LBA-04-13, LBA-03-21, LBA-03-05, LBA-98-120, LBA-01-14, LBA-02-23, LBA-02-22
[b]Outliers include LBA-03-14, LBA-03-15, LBA-04-13, LBA-03-21, LBA-03-05, LBA-02-23, LBA-02-22

inheritance (Douglass et al., 2005). The glacial system at Fachinal was an order of magnitude smaller and the advances were much shorter-lived than the massive ice lobes that discharged into Argentina, both of which lead to less landscape erosion, less erosion of boulders incorporated into the ice, and hence a greater proportion of boulders with inherited isotopes in the end moraine.

Data from Marine Isotope Stage 6 and older moraines at LBA (Kaplan et al., 2005) show even higher rates of exhumation (18%, as opposed to 14% for the LGM boulders), indicating that over longer time periods, more boulders have been exhumed or rolled from their original position. This is corroborated with plateaus in the accumulation of carbonate and clay-sized particles in local soils that may be caused by slow or episodic soil erosion (Douglass and Bockheim, 2006).

Even after the exclusion of the seven young outliers, there is still some spread in the ages within each moraine (Fig. 4, Table 2). For example, the oldest sample on Fenix III has an age of 22.1 ± 1.9 ka and is 2 ka older than the next oldest sample $(20.1 \pm 1.5$ ka), but because of the analytical uncertainty, this difference is not statistically significant at the 95% confidence limit. Also, the variability seen in the sample population is not significantly larger than what is expected based on the given uncertainties (the result of the χ^2 test). In the absence of any statistical basis for including or excluding particular samples, there could be nearly endless debate about whether this older sample has a small amount of inherited isotope, or whether all of the other boulders sampled on this moraine were exhumed a few thousand years after deposition. Increasing the number of analyses on these moraines would improve the MSWD statistics and the uncertainties in the weighted-mean age, but would likely not facilitate the conclusive rejection of these pseudo-outliers because their ages are statistically indistinguishable from the other boulder ages. We argue that all samples that share a common age should be incorporated into calculation of the moraine age (i.e., an average), and that unless there is a compelling reason to do so, there should not be any bias toward either younger or older samples.

5.2. Accuracy of cosmogenic isotope production rates

The uncertainties in scaling factors used to calculate isotope production rates are on the order of 10–20% (Gosse and Phillips, 2001). However, several lines of geologic evidence indicate that the production rates and scaling factors of Stone (2000) are accurate for southern South America. First, a local, long-term calibration site for ^{3}He showed that spallation reaction production rates for ^{3}He over the last 109 ka were only 11% higher than the global production rates determined for locations in North America (Ackert et al., 2003). This higher rate was attributed to a northward migration of the Antarctic Polar Front during glacial periods, which resulted in a drop in air pressure and an increase in production rates at 47°S, as well as magnetic field corrections. We expect a smaller correction for these younger samples because the lower air pressures experienced during glacial conditions would only apply for about half of their exposure history, and these samples were not exposed during the Mono Lake and Laschamp magnetic excursions when production rates were higher. This is significantly less than the positive 30% production rate anomaly over southern South America suggested by Pigati and Lifton (2004) (note these authors used different scaling factors and reconstructions of past magnetic fields in their study). Second, the ages of the Fenix I and Menucos moraines $(15.8 \pm 0.6$ and 14.4 ± 0.9 ka) straddle the AMS radiocarbon age of 15.2 ± 0.5 cal ka from the stratigraphically intervening carbonate concretions (Fig. 2). Even though it is possible that dead carbonate derived from pre-Quaternary rocks in the basin was incorporated into these concretions, this radiocarbon age does serve as an upper limit for the age of the Menucos moraine. Therefore, the actual production rates in this area

cannot be more than 10% lower than the calculated rates we have applied over the last 15 ka. Third, a parallel study of glacial advances in the Strait of Magellan using these same production rates and scaling factors obtained excellent agreement between cosmogenic nuclide and radiocarbon-based ages for several glacial deposits, thereby corroborating the accuracy of these factors over the last 25 kyr (McCulloch et al., 2005b). For these reasons, we infer that the actual uncertainties in cosmogenic nuclide production rates are less than ±10% in southernmost South America. For reference, a 10% uncertainty in P (Eq. (1)) propagates to 1580 years of additional uncertainty in the age of the 15.8 ka Fenix I moraine and would have little, if any, impact on paleoclimatic interpretations (below).

5.3. Paleoclimate implications of the LBA glacial chronology

The timing of the Last Glacial Maximum at LBA, 23–15 ka, is similar to glacial records in other parts of the world, despite a relative maximum in summer insolation at 46°S during this time interval (Fig. 5; Berger and Loutre, 1991). This supports prior assertions that at glacial to interglacial timescales, the Earth's climate behaves

synchronously (e.g., Denton et al., 1999a), and is tied to the global climate system (Sugden et al., 2005). However, at millennial time scales, the LBA glacial record maybe significantly different from those in other parts of South America (e.g., Denton et al., 1999b; McCulloch et al., 2005b). These differences are discussed below.

Perhaps the most significant finding is the 14.4±0.9 ka age of the Menucos moraine which places this last major advance of glaciers from the North Patagonia Ice Field within the early ACR and significantly predates the YD Chronozone. After deposition of the Menucos moraine, ice permanently retreated into the LBA basin, and there are no obvious moraines between the east end of the lake and the ca. 8.5 and 6.2 ka moraines at Fachinal (95 km to the west) that originated from a tributary valley. However, the geomorphic and stratigraphic relationships between the Fachinal moraines and the raised delta surface they rest upon suggest that the eastern side of the Northern Patagonian Ice Cap did not recede to the modern configuration until after ~6 ka (Douglass et al., 2005). Fourteen radiocarbon ages from paleo-lake shorelines and glacial deposits adjacent to Lago General Carerra, Chile (this body of water is contiguous with LBA, but has a different geographic name in Chile; Fig. 1), suggest that North Patagonia Ice Field glaciers retreated rapidly after
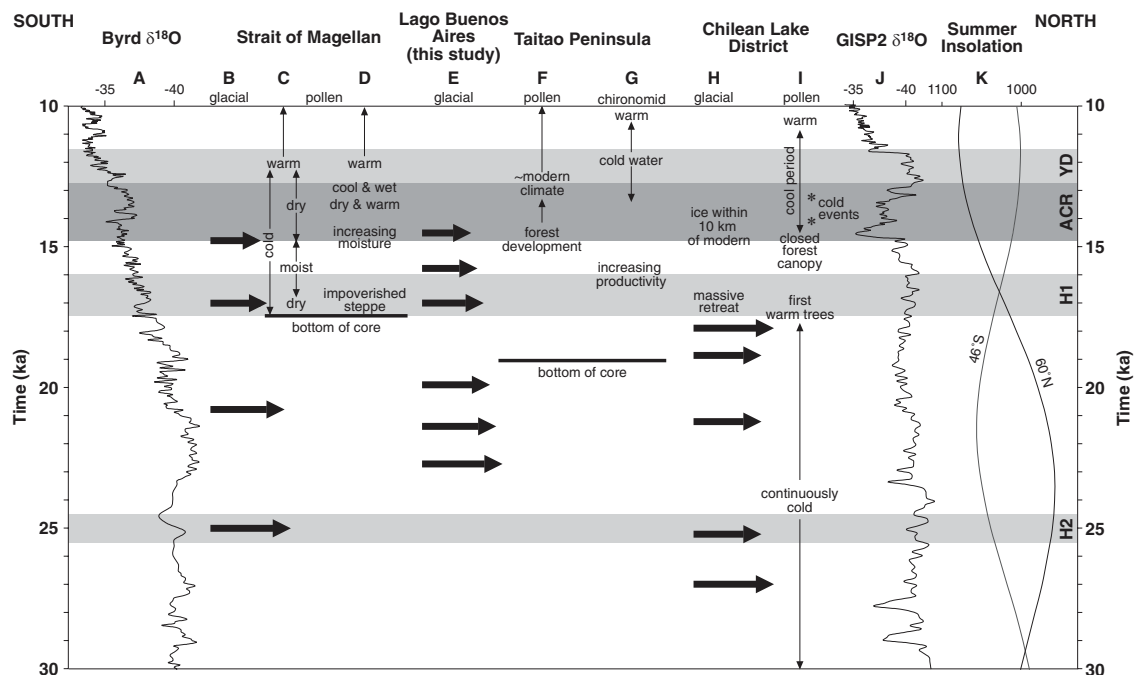

Fig. 5. Summary of glacial and paleoenvironmental records from southern South America and other parts of the world. From left to right: (A) oxygen isotope record from Byrd ice core, Antarctica, on the GISP2 timescale (Blunier and Brook, 2001), (B) timing of glacial advances in the Strait of Magellan (Kaplan et al., in prep; McCulloch et al., 2005b), (C) and (D) pollen interpretations from the Puerto del Hambre site, Strait of Magellan (Heusser et al., 2000; McCulloch and Davies, 2001, respectively), (E) glacial chronology from Lago Buenos Aires (this study), (F) pollen (Lumley and Switsur, 1993; Bennett et al., 2000) and (G) chironomid interpretations (Massaferro and Brooks, 2002) from the Taitao Peninsula and the Chonos archipelago, (H) glacial chronology (Denton et al., 1999b), (I) pollen interpretation (Moreno et al., 1999, 2001) from the Chilean Lake District, and (J) oxygen isotope record from the GISP2 ice core, Greenland (Blunier and Brook, 2001). (K) Summer insolation at 60°N (black) and 46°S (gray) (Berger and Loutre, 1991). The shaded boxes represent the timing of the Younger Dryas (YD), Antarctica Cold Reversal (ACR), and Heinrich Events 1 and 2 (H1, H2). For all records, the arrows represent the timing of glacial advances and the length of the arrow is proportional to the extent of the advance. The line underneath the paleoenvironmental records indicates the beginning of the record.

15–16 cal ka, and that the last high stand of LBA occurred 13.6–12.8 cal ka, and the lake drained suddenly to the Pacific Ocean ca. 12.8 cal ka, prior to the YD (Turner et al., 2005). These radiocarbon data are consistent with our cosmogenic nuclide chronology for the Fenix and Menucos moraines, but seem to conflict with details of the Holocene glacial chronology established at Fachinal, Chile (Douglass et al., 2005). Further dating of terraces and moraines west of Fachinal will be required to address this issue.

With the improved precision of moraine ages at LBA, we can now explore in detail the millennial-scale similarities and differences between this record and the well-resolved glacial and climate records from other parts of southern South America.

5.3.1. Taitao Peninsula

Pollen and other paleoecological records from the Taitao Peninsula and other islands in the Chonos archipelago (Fig. 1 inset; Fig. 5) provide a climate record from the opposite side of the Andes (Lumley and Switsur, 1993; Bennett et al., 2000; Massaferro and Brooks, 2002). Basal radiocarbon dates from these cores indicate that these low-lying areas became ice free between 16 and 18 cal ka. The pollen spectra from these cores show gradual changes in the vegetation between the time of deglaciation and the establishment of vegetation similar to modern at ca. 13 cal ka (Lumley and Switsur, 1993; Bennett et al., 2000). Analysis of *chironomid* (midge) capsules from one of these cores (Laguna Stibnite) provides a similar paleobiological record, but one taxon that typically occurs in glacier-fed lakes is consistently present between 13 and 10.6 cal ka and is interpreted to represent cooler temperatures during this interval (Massaferro and Brooks, 2002). This cold reversal was not identified in the pollen data, suggesting that either the vegetation did not respond to a climate change at this time, or that the changes in the *chironomid* taxa was not induced by climate change; however, three cosmogenic nuclide surface exposure ages from moraines east of the Northern Patagonian Ice Field suggest that ice margins stabilized between 12 and 10 ka (Glasser et al., 2006).

Despite their close proximities, the paleoclimate interpretations from opposite sides of the Andes are quite different. In the east, ice retreated from maximum positions between two and four thousand years after those glaciers in the west. Also, neither the pollen nor the *chironomid* paleoclimate proxies indicate cooler temperatures during the time of the Menucos advance (ca. 14.4 ka). This finding is highly unusual as the climate of southern South America is considered to be highly zonal, i.e. all weather is derived form the position and strength of the Southern Westerlies. The fact that we see different glacier responses at the same latitude indicates that the Andean Cordillera acts as an important climate boundary between these two locations.

5.3.2. Chilean Lake District

The glacial and pollen records from the CLD (Fig. 1 inset; Fig. 5) are supported by dozens of radiocarbon dates from numerous stratigraphic sections and cores (Lowell et al., 1995; Denton et al., 1999b; Moreno et al., 1999, 2001; Heusser et al., 1999). The glacial record indicates that ice advanced at ca. 35 and ca. 31 cal ka, but these deposits were overrun by a major advance at ca. 27 cal ka. This major advance was followed by less extensive advances at ca. 25, 21.3, and 18.8 cal ka. At ca. 17.9 cal ka, another large advance occurred, which overran the ca. 27 cal ka deposits in the southern parts of the CLD. It could not be determined how far the glaciers receded between these various advances, but pollen records indicate that climate was cold throughout the interval between 35 and 17.9 cal ka. At this time, there was major warming, and ice retreated approximately 90 km to within 10 km of the modern ice margins by 14.3 cal ka. However, there is indirect evidence of a glacial readvance during the late-glacial near the CLD as recorded by an increase in fine silt in lake cores from Lago Mascardi (Fig. 1 inset; Ariztegui et al., 1997; Hajdas et al., 2003). Pollen records indicate that trees representing warm conditions had moved into this area by 17.4 cal ka and that a full forest canopy existed between 16.0 and 14.2 cal ka. There was a reversal of this warming between 14.2 and 11.2 cal ka—the Huelmo-Mascardi Cold Period—with cold events at 14.2 and 13.3 cal ka. This cold period begins at the end of the ACR, i.e., before the start of the YD, and appears to be intermediate between the Antarctic and Greenland climate records. It is estimated that the temperatures during this late-glacial cool interval were ~3 °C lower than modern, compared to ~6 °C at the glacial maximum (Moreno et al., 2001).

There are two noticeable differences between the LBA and CLD glacial and climate records. First, the local glacial maximum at LBA occurs about 4 ka after the large 27 ka advance in the CLD. Ice advances at LBA may have been delayed by deep water in the lake basin. LBA is the deepest lake in South America (Murdie et al., 1999); water depths average ~400 m and approach 600 m in places. During glacier advances, the modern lake outlet was dammed, forcing water levels an additional ~230 m higher. A wide calving front (5–30 km wide, averaging ~10 km) may have posed a major impediment to ice advance. Glaciers in the CLD were advancing into shallower water bodies that would have posed less of an obstacle to ice advance. The extent of ice at LBA prior to ca. 22.7 ka cannot be determined; so it is possible that the earliest advances during MIS-2 were overrun by later, more extensive advances. Second, at the time of the last extensive advance at LBA (i.e., the Menucos moraine), glaciers in the CLD had dramatically retreated and were close to within 10 km of the modern ice margins. It is possible that the Menucos moraine correlates to the Huelmo-Mascardi cold period; however, the magnitudes of these events are very different. The best interpretation is that the Southern

Westerlies had migrated south of 41°S by the late-glacial time, reducing the amount of water available for glacier growth. As there are several lines of evidence that suggest that the chronological differences between the CLD and LBA are not related to incorrect cosmogenic isotope production rates, we conclude that significant differences in climate and/or ice dynamics allowed glaciers to persist much longer at LBA than in the CLD.

5.3.3. Strait of Magellan

Moraines and peat bogs around the Strait of Magellan have also provided detailed climate records for the last glaciation (Fig. 1 inset; Fig. 5). Early radiocarbon-based glacial chronologies from this area indicated that glaciers advanced much earlier here than in other parts of southern South America (Clapperton et al., 1995); however, it is now thought that many of the samples were contaminated by dead carbon from lignite bedrock sources. More recent chronologies based on [10]Be surface exposure dating and lignite-free radiocarbon samples (McCulloch et al., 2005b) give ages of ca. 25–23, 21, and 17 cal ka for four advances during the Last Glacial Maximum in the Strait of Magellan. Jackofsky (2001) also reports [10]Be surface exposure ages of ~20 ka from eight boulders in this area, but it is not clear if these samples come from the same moraine as the ~21 ka moraine of McCulloch et al. (2005b). After ca. 17 cal ka, the glacier occupying the Strait of Magellan retreated, allowing a proglacial lake to drain (McCulloch and Davies, 2001). The lake reformed between 14.9 and 12 cal ka (McCulloch et al, 2005a), and was likely coeval with a 13.2 ± 1.6 ka advance near Torres del Paine (Fig. 1 inset; Fogwill and Kubik, 2005). Interpretations of the pollen records from Puerto del Hambre (Heusser et al., 2000; McCulloch and Davies, 2001) and other locations (Heusser, 1998) are slightly different during the late-glacial interval, but it is clear that the vegetation at this time was quite variable. However, both records show that a slight warming started ca. 12.5 cal ka (note that this is before the end of the YD Chronozone), and that conditions similar to the modern climate were reached by ca. 10.5 cal ka.

The Strait of Magellan record is quite similar to the LBA record. Maximum ice extent at the Strait of Magellan (25 ka) preceded the maximum extent at LBA (22.7) by about 2 ka, but this can be explained by more intensive calving in the deeper water at LBA. During the last glaciation, average water depths in LBA were ~600 m, and only ~400 m in the Strait of Magellan. Ice damming increased the water depth in LBA, whereas lower eustatic sea level contributed to shallower water in the Strait of Magellan. After this, both records are similar, with glacial advances at ca. 20, 17, and 14.5 ka. However, we note there is no equivalent to the Fenix I moraine (15.8 ka) in the Strait of Magellan. Most importantly glacier advances occurred in both the Strait of Magellan and LBA during the time of the ACR, and there is no evidence of advances persisting through the end of the YD at either location.

6. Conclusions

The MSWD statistic and cumulative frequency plots are useful tools for identifying geologic outliers in cosmogenic nuclide surface exposure data. For the last-glacial moraines at Lago Buenos Aires (LBA), seven of 49 samples are identified as anomalously young and are interpreted as exhumed boulders. No samples are unusually old. Moraine ages based on the arithmetic mean of boulder ages are not significantly different from those based on the inverse-variance weighted mean of boulder ages; however, the weighted-mean ages are more precise. We prefer the weighted-mean age of the boulders as the best estimate for moraine age because most of the non-analytical error is removed from the data by the identification of geologic outliers.

This glacial record is broadly similar to other glacial and paleoclimate records in southern South America, and in other parts of the world. At LBA, the maximum ice extent was reached at ~23 ka, despite a maximum in summer insolation at this time. This is somewhat later than the maximum ice extent in the Strait of Magellan and significantly later than the Chilean Lake District (CLD). Some of these differences might be explained by local ice dynamics, e.g., the late maximum extent of ice at LBA might be related to a wide calving ice margin as the ice advanced through the LBA basin. At LBA, deglaciation was interrupted by a late-glacial readvance at 14.4 ± 0.9 ka, which is contemporaneous with the Antarctic Cold Reversal (ACR), and significantly earlier than the Younger Dryas (YD). Similar advances are seen in the Strait of Magellan area (McCulloch et al., 2005b), near Torres del Paine (Fogwill and Kubik, 2005), and in New Zealand (e.g., Turney et al., 2003). The Huelmo-Mascardi cold event in the CLD appears to be intermediate between an ARC and YD-type cooling event (Sugden et al., 2005). Regional climatic differences in southern South America are likely related to the strength and position of the Southern Westerlies; however, the distinctly different climates on opposite sides of the Andes at 46°S indicate that the Andes may affect otherwise zonal circulation patterns.

Acknowledgments

would not be possible without the logistical support and friendship of R. and J. Nauta of Estancia Telken, and the cooperation of E.D. Azpillaga and G. DeLanger of Estancia Page Chico, and L. Perez of Estancia La Margarita.

References

Ackert, R.P., Singer, B.S., Guillou, H., Kaplan, M.R., Kurz, M.D., 2003. Long-term cosmogenic ^{3}He production rates from ^{40}Ar/^{39}Ar and K-Ar dated Patagonian lava flows at 47°S. Earth and Planetary Science Letters 210, 119–136.

Ariztegui, D., Bianchi, M.M., Massaferro, J., Lafargue, E., Niessen, F., 1997. Interhemispheric synchrony of Late-glacial climatic instability as recorded in proglacial Lake Mascardi, Argentina. Journal of Quaternary Science 12, 333–338.

Bennett, K.D., Haberle, S.G., Lumley, S.H., 2000. The Last Glacial–Holocene transition in southern Chile. Science 290, 325–328.

Benson, L., Madole, R., Landis, ., Gosse, J., 2005. New data for Late Pleistocene Pinedale alpine glaciation from southwestern Colorado. Quaternary Science Reviews 24, 49–65.

Berger, A., Loutre, M.F., 1991. Insolation values for the climate of the last 10 million years. Quaternary Sciences Reviews 10, 297–317.

Bierman, P.R., Caffee, M.W., Davis, P.T., Marsella, K., Pavich, M., Colgan, P., Mickelson, D., Larsen, J., 2002. Rates and timing of Earth surface processes from in situ-produced cosmogenic Be-10. In: Grew, E.S. (Ed.), Beryllium: Mineralogy, Petrology, and Geochemistry: Reviews in Mineralogy and Geochemistry, vol. 50. pp.147–205.

Blunier, T., Brook, E.J., 2001. Timing of millennial-scale climate change in Antarctica and Greenland during the last glacial period. Science 291, 109–112.

Bond, G., Kromer, B., Beer, J., Muscheler, R., Evans, M.N., Showers, W., Hoffmann, S., Lotti-Bond, R., Hajdas, I., Bonani, G., 2001. Persistent solar influence on North Atlantic climate during the Holocene. Science 294, 2130–2136.

Broecker, W.S., Denton, G.H., 1989. The role of ocean-atmosphere reorganizations in glacial cycles. Geochimica et Cosmochimica Acta 53, 2465–2501.

Brook, E.J., Brown, E.T., Kurz, M.D., Raisbeck, G., Yiou, F., 1996. An Antarctic perspective on in-situ cosmogenic nuclide production. Radiocarbon 38, 150.

Brook, E.J., Harder, S., Severinghaus, J., Bender, M., 1999. Atmospheric methane and millennial-scale climate change. In: Clark, P., et al. (Eds.), Mechanisms of Global Climate Change at Millennial Time Scales: American Geophysical Union Geophysical Monograph 113. pp. 165–175.

Caldenius, C.G., 1932. Las glaciaciones Cuaternarias en la Patagonia y Tierra del Fuego. Geografiska Annaler 14, 1–164.

Cane, M., Clement, A., 1999. A role for the tropical Pacific coupled ocean-atmosphere system on Milankovitch and millennial timescales: part II Global impacts. In: Clark, P., et al. (Eds.) Mechanisms of Global Climate Change at Millennial Time Scales: American Geophysical Union Geophysical Monograph 113. pp. 373–383.

Clapperton, C.M., Sugden, D.E., Kaufman, D.S., McCulloch, R.D., 1995. The last glaciation in Central Magellan Strait, southernmost Chile. Quaternary Research 44, 133–148.

Dalrymple, G.B., Lanphere, M.A., 1969. Potassium–Argon Dating. W. H. Freeman, San Francisco, CA, 258pp.

Deino, A., Potts, P., 1992. Age-probability spectra for for examination of single-crystal ^{40}Ar/^{39}Ar dating results: examples from Olorgesailie, southern Kenyan rift. Quaternary International 13/14, 47–53.

Denton, G.H., Heusser, C.J., Lowell, T.V., Moreno, P.I., Anderson, B.G., Heusser, L.E., Schlüchter, C., Marchant, D.R., 1999a. Interhemispheric linkage of paleoclimate during the last glaciation. Geografiska Annaler 81A, 107–153.

Denton, G.H., Lowell, T.V., Heusser, C.J., Schlüchter, C., Andersen, B.G., Heusser, L.E., Moreno, P.I., Marchant, D.R., 1999b. Geomorphology, stratigraphy, and radiocarbon chronology of Llanquihue drift in the area of the southern Lake District, Seno Reloncaví, and Isla Grande de Chiloé, Chile. Geografiska Annaler 81A, 167–229.

Douglass, D.C., Bockheim, J.G., 2006. Soil-forming rates and processes on Quaternary moraines near Lago Buenos Aires, Argentina. Quaternary Research 65, 293–307.

Douglass, D.C., Singer, B.S., Kaplan, M.R., Ackert, R.P., Mickelson, D.M., Caffee, M.W., 2005. Evidence of early Holocene glacial advances in southern South America from cosmogenic surface-exposure dating. Geology 33, 237–240.

Dunne, A., Elmore, D., Muzikar, P., 1999. Scaling factors for the rates of production of cosmogenic nuclides for geometric shielding and attenuation at depth on sloped surfaces. Geomorphology 27, 3–11.

Finkel, R.C., Suter, M., 1993. AMS in the Earth sciences: technique and applications. In: Hyman, M., Rowe, M.W. (Eds.), Advances in Analytical Geochemistry, vol. 1. pp. 1–114.

Fogwill, C.J., Kubik, P.W., 2005. A glacial stage spanning the Antarctic Cold Reversal in Torres del Paine (51°S), Chile, based on preliminary cosmogenic exposure ages. Geografiska Annaler 87A, 403–408.

Glasser, N.F., Harrison, S., Ivy-Ochs, S., Duller, G.A.T., Kubik, P.W., 2006. Evidence from the Rio Bayo valley on the extent of the North Patagonian Icefield during Late Pleistocene–Holocene transition. Quaternary Research 65, 70–77.

Gosse, J.C., Phillips, F.M., 2001. Terrestrial in situ cosmogenic nuclides: theory and application. Quaternary Science Reviews 20, 1475–1560.

Gosse, J.C., Evenson, E.B., Klein, J., Lawn, B., Middleton, R., 1995. Precise cosmogenic ^{10}Be measurements in western North America: support for a global Younger Dryas cooling event. Geology 23, 877–880.

Gosse, J.C., Evenson, E., Klein, J., Sorenson, C., 2003. Cosmogenic nuclide glacial geochronology in the Wind River Range, Wyoming. In: Easterbrook, D.J. (Ed.), Quaternary Geology of the United States, INQUA 2003 Field Guide Volume. Desert Research Institute, Reno, NV, pp. 49–56.

Guyodo, Y., Valet, J.P., 1999. Global changes in intensity in the Earth's magnetic field during the past 800 kyr. Nature 399, 249–252.

Hajdas, I., Bonani, G., Moreno, P.I., Ariztegui, D., 2003. Precise radiocarbon dating of Late-Glacial cooling in mid-latitude South America. Quaternary Research 59, 70–78.

Heusser, C.J., 1998. Deglacial paleoclimate of the American sector of the Southern Ocean: Late Glacial–Holocene records from the latitude of Canal Beagle (55°S), Argentine Tierra del Fuego. Palaeogeography, Palaeoclimatology, Palaeoecology 141, 277–301.

Heusser, C.J., Heusser, L.E., Lowell, T.V., 1999. Paleoecology of the southern Chilean Lake District–Isla Grande de Chiloé during middle–late Llanquihue glaciation and Deglaciation. Geografiska Annaler 81A, 231–284.

Heusser, C.J., Heusser, L.E., Lowell, T.V., Moreira, A., Moreira, M.S., 2000. Deglacial paleoclimate at Puerto del Hambre, subantarctic Patagonia, Chile. Journal of Quaternary Science 15, 101–114.

Holden, N.E., 1990. Total half-lives for selected nuclides. Pure and Applied Chemistry 62, 941–958.

Inbar, M., Ostera, H.A., Parica, C.A., Remesal, M.B., Salani, F.M., 1995. Environmental assessment of 1991 Hudson volcano eruption ashfall effects on southern Patagonia region, Argentina. Environmental Geology 25, 119–125.

Ivy-Ochs, S., Schlüchter, C., Kubik, P.W., Denton, G.H., 1999. Moraine exposure dates imply synchronous Younger Dryas glacier advances in the European Alps and in the Southern Alps of New Zealand. Geografiska Annaler 81A, 313–323.

Jackofsky, D.S., 2001. Quaternary Glacial Chronology and Climate Dynamics in Tierra del Fuego, Chile and at Lago Nahuel Huapi, Argentina. M.S. Thesis, University of Kansas.

Kaplan, M.R., Ackert, R.P., Singer, B.S., Douglass, D.C., Kurz, M.D., 2004. Cosmogenic nuclide chronology of millennial-scale glacial

advances during O-isotope stage 2 in Patagonia. Geological Society of America Bulletin 116, 308–321.

Kaplan, M.R., Douglass, D.C., Singer, B.S., Ackert, R.P., Caffee, M.W., 2005. Cosmogenic nuclide chronology of pre-last glaciation maximum moraines at Lago Buenos Aires, 46°S, Argentina. Quaternary Research 63, 301–315.

Licciardi, J.M., Clark, P.U., Brook, E.J., Elmore, D., Sharma, P., 2004. Variable responses of western US glaciers during the last Deglaciation. Geology 32, 81–84.

Lowell, T.V., Heusser, .J., Andersen, B.G., Moreno, P.I., Hauser, A., Heusser, L.E., Schluchter, C., Marchant, D.R., Denton, G.H., 1995. Interhemispheric correlation of late Pleistocene glacial events. Science 269, 1541–1549.

Ludwig, K.R., 2003. Isoplot/Ex 3.00: A Geochronological Toolkit for Microsoft Excel. Berkeley Geochronology Center Special Publication No. 4, 70pp.

Lumley, S.H., Switsur, R., 1993. Late Quaternary chronology of the Taitao Peninsula, southern Chile. Journal of Quaternary Science 8, 161–165.

Marden, C.J., Clapperton, C.M., 1995. Fluctuations of the South Patagonian Ice-field during the last glaciation and the Holocene. Journal of Quaternary Science 10, 197–210.

Massaferro, J., Brooks, S.J., 2002. Response of chironomids to Late Quaternary environmental change in the Taitao Peninsula, southern Chile. Journal of Quaternary Science 17, 101–111.

McCulloch, R.D., Davies, S.J., 2001. Late-glacial and Holocene palaeoenvironmental change in the central Strait of Magellan, southern Patagonia. Palaeogeography, Palaeoclimatology, Palaeoecology 173, 143–173.

McCulloch, R.D., Bentley, M.J., Tipping, R.M., Clapperton, C.M., 2005a. Evidence for late-glacial ice dammed lakes in the central Straight of Magellan and Bahía Inútil, southernmost South America. Geografiska Annaler 87A, 335–362.

McCulloch, R.D., Fogwill, C.J., Sugden, D.E., Bentley, M.J., Kubick, P.W., 2005b. Chronology of the last glaciation in central Strait of Magellan and Bahía Inútil southernmost South America. Geografiska Annaler 87A, 289–312.

McDougall, I., Harrison, T.M., 1999. Geochronology and Thermochronology by the ^{40}Ar/^{39}Ar Method, second ed. Oxford University Press, Oxford, 269pp.

McIntyre, G.A., Brooks, C., Compston, W., Turek, A., 1966. The statistical assessment of Rb–Sr isochrones. Journal of Geophysical Research 71, 5459–5468.

Mercer, J.H., 1968. Variations of some Patagonian glaciers since the Late-Glacial. American Journal of Science 266, 91–109.

Mercer, J.H., 1976. Glacial history of southernmost South America. Quaternary Research 6, 125–166.

Moreno, P.I., Lowell, T.V., Jacobson, G.L., Denton, G.H., 1999. Abrupt vegetation and climate changes during the last glacial maximum and last termination in the Chilean Lake District: a case study from Canal de la Puntilla (41°S). Geografiska Annaler 81A, 285–311.

Moreno, P.I., Jacobson, G.L., Lowell, T.V., Denton, G.H., 2001. Interhemispheric climate links revealed by a late-glacial cooling episode in southern Chile. Nature 409, 804–808.

Murdie, R.E., Pugh, D.T., Styles, P., 1999. A lightweight, portable, digital probe for measuring the thermal gradient in shallow water sediments, with examples from Patagonia. Geo-Marine Letters 18, 315–320.

Muzikar, P., Elmore, D., Granger, D.E., 2003. Accelerator mass spectrometry in geologic research. Geological Society of America Bulletin 115, 643–654.

National Center for Atmospheric Research, 2003. World Monthly Surface Station Climatology, 1738–cont. ⟨http://dss.ucar.edu/datasets/ds570.0/⟩.

Nishiizumi, K., Winterer, E.L., Kohl, C.P., Klein, J., Middleton, R., Lal., D., Arnold, J.R., 1989. Cosmic ray production rates of ^{10}Be and ^{26}Al in quartz from glacially polished rocks. Journal of Geophysical Research B 94, 17907–17915.

Owen, L.A., Finkel, R.C., Haizhou, M., Spencer, J.Q., Derbyshire, E., Barnard, P.L., Caffee, M.W., 2003. Timing and style of Late Quaternary glaciation in northeastern Tibet. Geological Society of America Bulletin 115, 1356–1364.

Partridge, T.C., Granger, D.E., Caffee, M.W., Clarke, R.J., 2003. Lower Pliocene Hominid Remains from Sterkfontein. Science 300, 607–612.

Phillips, F.M., 2004. CRONUS-Earth (Cosmic-Ray Produced Nuclide Systematics on Earth) project: the start-up. Geological Society of America Abstracts with Programs 36, 531.

Pigati, J.S., Lifton, N.A., 2004. Geomagnetic effects on time-integrated cosmogenic nuclide production with emphasis on in situ ^{14}C and ^{10}Be. Earth and Planetary Science Letters 226, 193–205.

Putkonen, J., Swanson, T., 2003. Accuracy of cosmogenic ages for moraines. Quaternary Research 59, 255–261.

Reimer, P.J., Baillie, M.G.L., Bard, E., Bayliss, A., Beck, J.W., Bertrand, C., Blackwell, P.G., Buck, C.E., Burr, G., Cutler, K.B., Damon, P.E., Edwards, R.L., Fairbanks, R.G., Friedrich, M., Guilderson, T.P., Hughen, K.A., Kromer, B., McCormac, F.G., Manning, S., Bronk Ramsey, C., Reimer, R.W., Remmele, S., Southon, J.R., Stuiver, M., Talamo, S., Taylor, F.W., van der Plicht, J., Weyhenmeyer, C.E., 2004. IntCal04 Terrestrial Radiocarbon Age Calibration, 0–26 Cal Kyr BP. Radiocarbon 46, 1029–1058.

Singer, B.S., Ackert, R.P., Guillou, H., 2004. ^{40}Ar/^{39}Ar and K-Ar chronology of Pleistocene glaciations in Patagonia. Geological Society of America Bulletin 116, 434–450.

Steig, E.J., Brook, E.J., White, J.W.C., Sucher, C.M., Bender, M.L., Lehman, S.J., Morse, D.L., Waddington, E.D., Clow, G.D., 1998. Synchronous climate changes in Antarctica and the North Atlantic. Science 282, 92–95.

Stone, J.O., 2000. Air pressure and cosmogenic isotope production. Journal of Geophysical Research B 105, 23753–23759.

Strelin, J.A., Malagnino, E.C., 2000. Late-Glacial history of the Lago Argentino, Argentina, and age of the Puerto Bandera moraines. Quaternary Research 54, 339–347.

Sugden, D.E., Bentley, M.J., Fogwill, C.J., Hulton, N.J., McCulloch, R.D., Purves, R.S., 2005. Late-glacial glacier events in southernmost South America: a blend of 'northern' and 'southern' hemispheric climate signals. Geografiska Annaler 87, 273–288.

Taylor, J.R., 1997. An Introduction to Error Analysis. The Study of Uncertainties in Physical Measurements, second ed. University Science Books, Sausalito, CA, 327pp.

Turner, K.J., Fogwill, C.J., McCulloch, R.D., Sugden, D.E., 2005. Deglaciation of the eastern flank of the North Patagonian Icefield and associated continental-scale lake diversions. Geografiska Annaler 87A, 363–374.

Turney, C.S.M., McGlone, M.S., Wilmhurst, J.M., 2003. Asynchronous climate change between New Zealand and the North Atlantic during the last deglaciation. Geology 31, 223–226.

Weninger, B., Jöris, O., Danzeglocke, U., 2004. Radiocarbon calibration and paleoclimate research programme: CalPal2004. Colonge. Available at: ⟨http://www.calpal-online.de/⟩.

Wenzens, G., 1999. Fluctuations of outlet and valley glaciers in the southern Andes (Argentina) during the past 13,000 years. Quaternary Research 51, 238–247.

Zreda, M.G., Phillips, F.M., 1995. Insights into alpine moraine development from cosmogenic ^{36}Cl buildup dating. Geomorphology 14, 149–156.